SODIUM INACTIVATION IN NERVE FIBERS

ROSALIE C. HOYT

From the Department of Physics, Bryn Mawr College, Bryn Mawr, Pennsylvania 19010

ABSTRACT A number of models proposed to account for the sodium conductance changes are shown to fall into two classes. The Hodgkin-Huxley (HH) model falls into a class (I) in which the conductance depends on two or more independent variables controlled by independent processes. The Mullins, Hoyt, and Goldman models fall into class II in which conductance depends directly on one variable only, a variable which is controlled by two or more coupled processes. The HH and Hoyt models are used as specific examples of the two classes. It is shown that, contrary to a recently published report, the results from double experiments can be equally well accounted for by both models. It is also shown that steady-state conditioning, or "inactivation," curves, obtained at more than one test potential, can be used to distinguish the two models. The HH equations predict that such curves should be shifted, by very small amounts, in the hyperpolarizing direction when more depolarizing test potentials are used, while the Hoyt model predicts that they should be shifted in the depolarizing direction, by quite appreciable amounts. Several pieces of published experimental information are used as tests of these predictions, and give tentative support to the class II model. Further experiments are necessary before a definite conclusion can be reached.

I. INTRODUCTION

A number of different models have been suggested to account for the observed changes in the conductance of the "early" channel, here for convenience called the sodium channel. The term model is used here in a very general sense, and includes both purely mathematical models in which the phenomena are merely correlated by means of equations, and models in which specific physicochemical mechanisms are postulated to account for the phenomena. Mathematically, a number of these models (1–4) may be divided into two classes (Fig. 1). In one type (I) it is assumed that the sodium conductance, g_N, depends on two or more *independent variables*, $a, b, \cdots$, and that the instantaneous values of these variables are determined by *independent processes*, $P_a, P_b, \cdots$. As a result of the independence of the variables the sodium conductance is given as a separated product of single variable functions. In the other type (II) it is assumed that g_N is a function of only *one variable*, x, but that the instantaneous value of this one variable is determined by two or more *coupled processes*, $P_1, P_2, \cdots$.

As noted in Fig. 1, the model of Hodgkin and Huxley (1) belongs to class I, while those of Mullins (2), Hoyt (3), and Goldman (4)[1] belong to class II. In the HH model, the m and h processes given by equations 2 and 3 in Fig. 1 are independent of each other. In the Hoyt model, as a result of the coupling term $k_1(w - w_\infty)$, the process of equation 5 is not independent of the process of equation 4, and both processes determine the single variable v.[2] In the Mullins model, the single variable determining the sodium conductance is the number of unblocked pores of the right size. This number is determined by three *coupled* processes, the unblocking of pores, the change of size of unblocked pores, and the reblocking of pores. Similarly, in the Goldman model the single variable is the number of dipoles

(I) Independent Variables, Independent Processes (Hodgkin and Huxley)

$g_N = f_1(a) \cdot f_2(b) \ldots$ (HH) $g_N = \bar{g} m^3 h$ (1)

$a = a(P_a)$ $\dot{m} = \alpha_m - (\alpha_m + \beta_m)m$ (2)

$b = b(P_b)$ $\dot{h} = \alpha_h - (\alpha_h + \beta_h)h$ (3)

(II) Single Variable, Coupled Processes (Mullins, Hoyt, Goldman)

$g_N = f(x)$

$x = x(P_1, P_2, \ldots)$

(Hoyt) $g_N(v)$ v

$\dot{w} = -k_1(w - w_\infty)$ (4)

$\dot{v} = -k_1(w - w_\infty) - k_3(v - v_\infty)$ (5)

FIGURE 1 The two model classes. The general characteristics of each class are given at the left. For each class a specific example is indicated at the right.

in the orientation that preferentially binds sodium. This number is determined by the coupled processes of binding and unbinding of ions and reorientations of the flexible dipoles. (See equations 2–6, inclusive of Goldman (4).)

It is worth noting at this point that by modification of the underlying assumptions, the physical model suggested by HH (1) may be converted from class I to class II.

---

[1] Since this paper is concerned with the sodium conductance only, we ignore the fact that in both the Mullins and Goldman models the kinetics of the sodium channel are further coupled to those of the potassium channel.

[2] The variable u of reference 3 has been replaced by the variable $w = -u$ throughout this paper.

For example, one might postulate that the single inactivating site cannot be occupied until all three activating sites have been occupied. As a result, the variable h will no longer be independent of the variable m, and the h process of equation 3 (Fig. 1) will have to include a coupling term that involves m. Further, the Mullins (2) model may be converted from class II to class I by assuming, for example, that change in pore size proceeds independently of unblocking.

Since the two model classes are qualitatively quite different in mathematical nature, one would intuitively expect quantitative differences to arise when models from the two classes are used to predict results covering a wide range of phenomena. Yet an earlier analysis (3) seemed to indicate that the Hodgkin and Huxley example of class I, I-HH, and the Hoyt example of class II, II-H, were equally successful in predicting results in agreement with experiment. More recently, experimental results have been presented by Chandler, Hodgkin, and Meves (5) which the authors show to be in agreement with the predictions of I-HH, but which they contend are in disagreement with those of II-H. However, the latter conclusion is not justified. A more complete analysis, presented in section II of this paper, shows that the predictions of the II-H model are also in good quantitative agreement with the specific experimental data presented by Chandler, Hodgkin, and Meves. A further search must be made for an experimental test of the relative validity of models from the two classes. Additional analyses have now shown that conditioning experiments, carried out at different test clamp voltages as well as at different preclamp voltages, may provide a sensitive tool for distinguishing between the two classes. The results of these analyses, as applied specifically to the I-HH and II-H models are presented in section III, where it is shown that the predictions of the two models are quite different. It is also shown that the existing relevant experimental data as published in the literature, while meager, gives some support to the II-H model. Finally, in section IV an attempt is made to draw more general conclusions as to the expected behavior of models from the two classes.

II. A DOUBLE PULSE EXPERIMENT

In the experiment illustrated in Fig. 5 of the paper by Chandler, Hodgkin, and Meves (5), a squid axon, internally perfused with a solution of 300 mM RbCl + sucrose, was held at a potential of -60 mv and then pulsed to a potential of $+10$ mv. The temperature was 0°C. The resulting inward sodium current followed the time course shown by the circles at the top of Fig. 2. According to the I-HH model, the initial phase of this negative current results from the increase of m with time and the declining phase from the decrease of h with time. The authors did not try to fit the m kinetics to the initial phase of the current. The solid exponential curve, representing the fit of the h dependence to the declining phase, requires that the HH parameter τ_h be assigned the value 6.2 msec for the test voltage of $+10$ mv. However, the HH equations, when scaled to a temperature of 0°C (equations

4–6 of reference 5) predict that for a clamp to +10 mv the value of τ_h should be close to 2 msec. No explanation is given by the authors for the much larger than expected value of τ_h.

When the II-H model is fitted to the same single clamp results, the dashed curve shown at the top of Fig. 2 is obtained. During the falling phase the two models are in essentially complete agreement. Some of the details of the calculations that were performed in order to obtain this dashed curve are given in the Appendix. Here we give a more qualitative discussion of why such a current-time curve is to be expected from this model. As noted in Fig. 1, the sodium conductance, g, is assumed to depend in a monotonic fashion on a variable v. The dependence of g on v in Fig. 1 is similar to the power law dependences, n^4, m^3, of the HH model. Tabular values for $g(v)$ are given in Table II of the Appendix. The instantaneous value of g

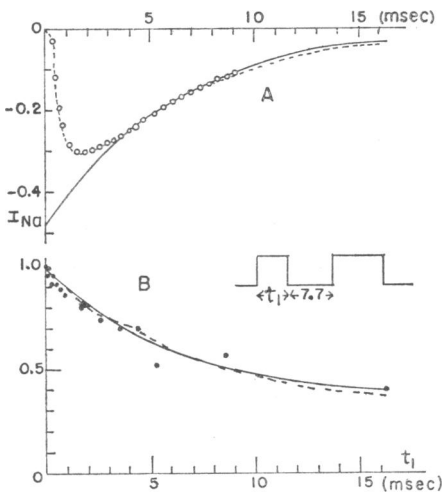

FIGURE 2 Experiment of Chandler, Hodgkin, and Meves (5). External solution; K-free ASW. Internal perfusate: 300 mM RbCl + sucrose. Resting potential = −40 mv; holding potential = −60 mv. (*A*) Inward current vs. time from start of depolarizing pulse to +10 mv. Continuous curve, $-0.485 \exp(-t/6.2)$. Dashed curve, fit of the Hoyt model where it departs from the continuous curve. (*B*) Ratio of peak current in second pulse to that of (*A*). Pulse arrangement shown in inset. Smooth curve, fit of the HH model. Dashed curve, fit of the Hoyt model.

is thus given by the instantaneous value of v. These instantaneous values of v are determined by the equations

$$\dot{w} = -k_1(w - w_e) \tag{4}$$

$$\dot{v} = -k_1(w - w_e) - k_3(v - v_e) \tag{5}$$

where w_e and v_e are voltage-dependent equilibrium values of w and v, and k_1 and k_3 are voltage-dependent rate constants.

The time dependences of w and v, for a depolarizing clamp starting at $t = 0$, are shown in Fig. 3*A*. According to equation 4, w undergoes a simple exponential increase from its initial value, w_0, to its final value, w_e,

$$w = w_e - (w_e - w_0) \exp(-k_1 t).$$

If the second term in equation 5 were *not* present, v would undergo an identical, but displaced, simple exponential increase from its small initial value, v_0, dashed curve. However, the presence of the term $k_3(v - v_e)$ eventually causes v to decrease to its new small equilibrium, v_e. The latter decrease is described by an exponential term, $\exp(-k_3 t)$. Once the time dependence of v is determined, the corresponding time dependence of the conductance g, Fig. 3*B*, is obtained from the monotonic $g(v)$ function. Finally, multiplication of the $g(t)$ curve by the driving force, $(E - E_{Na})$, leads to the dashed curve shown at the top of Fig. 2.

As in the I-HH case, in order to obtain the dashed curve of Fig. 2, one parameter of the II-H model, k_3, had to be given a value ($k_3 = 0.13$ msec^{-1}) quite different from that expected at +10 mv and 0°C ($k_3 = 0.42$ msec^{-1}). It is not obvious why such parameter changes are required of *both* models. That the low temperatures used are the cause would seem unlikely. Experimental evidence is quite good for the customary usage of a Q_{10} of 3 when converting various nerve fiber rate constants

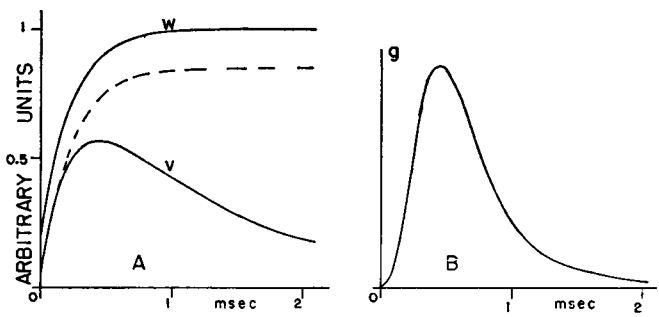

FIGURE 3 Voltage clamping in the II-H model. (*A*) Time dependence of v and w, equations 4 and 5. The dashed curve shows the variation in v that would occur in the absence of the coupling of v to w in equation 5. (*B*) Time dependence of the sodium (early) conductance.

experimentally determined at one temperature to those appropriate for another temperature. For perfused fibers, Fig. 3 of Chandler, Hodgkin, and Meves (5) shows that for membrane voltages in the range −100 to −40 mv such scaling of τ_h is experimentally valid down to temperatures of 0°C ± 1°C. It is therefore improbable that the low temperatures (0°C) used in this experiment can account for the anomalously large values for τ_h and k_3 apparently required here at a membrane voltage of +10 mv. Other possible reasons for these anomalous parameter values include effects due to the perfusion process itself, the presence of internal Rb rather than K, and of the large internal Cl concentration used. However, if freedom of choice of parameters is allowed to both models, they are equally capable of providing good fits to the single clamp data.

In the second half of their experiment Chandler, Hodgkin, and Meves applied two pulses, from −60 to +10 mv, in succession, as shown in the inset in Fig. 2. The duration of the interval between pulses was maintained at the constant value

of 7.7 msec, while the duration of the first pulse, t_1, was varied. The ratios of the peak sodium currents during the second pulse to that obtained with no prepulse are shown by the experimental points in the lower half of Fig. 2. These ratios are seen to decrease as the duration of the first pulse is increased.

According to the I-HH model the peak sodium current during the second pulse is almost strictly proportional to the value of h at the start of the second pulse. With a fixed recovery interval between pulses, h at the start of the second pulse will depend exponentially on the duration of the first pulse. Using the same (anomalous) value of τ_h at +10 mv as determined in the upper curve (6.2 msec), and a value of $\tau_h = 18.5$ msec for the recovery interval at −60 mv, the HH model predicts that the peak current ratios should approximately be given by

$$0.34 + 0.66 \exp(-t_1/6.2),$$

which is shown by the solid curve. This prediction is seen to be in reasonable agreement with the experimental points.

Application of the II-H model to this experiment has been made using, for +10 mv, the same values of the parameters as used in the upper curve and for −60 mv, the parameters shown in Table IV of the Appendix. This choice leads to predicted peak current ratios given by the dashed curve, in equally as good agreement with the experimental points as the solid curve.[3] The Chandler, Hodgkin, and Meves (5) statement for the II-H model, that the "rate of inactivation during the first pulse was proportional to the sodium conductance," is therefore seen not to be true for the II-H model in general. As will become clearer in the next section, no such simple explanation can be given to "inactivation" in class II models. However, it is true that, unlike the prediction of the HH model which requires an exponential curve, in the II-H model the shape of the dashed curve in the lower half of Fig. 2 is qualitatively dependent on the choice of the parameters. A parameter choice could have been made such that the curve would start off with close to a zero slope at $t_1 = 0$, as drawn by Chandler, Hodgkin, and Meves. However, for the parameters chosen, forced in part by the fit to the curve in the upper half of the figure, the predicted dashed curve does not lead to this zero initial slope.

From the above analyses one may conclude that experiments using only one holding potential and one test potential may never provide a sufficiently sensitive test to distinguish between the I-HH and II-H models. Both models have four parameters dependent on the membrane potential difference, (m_e, h_e, τ_m, τ_h) and (k_1, k_3, w_e, v_e). In each model these parameters can be adjusted to fit the environmental conditions and this freedom may often eliminate the possibility of a crucial test. On the other hand, the assumed uniqueness for both models of their parameter dependences on membrane potential, for given, fixed environmental conditions,

[3] The details of the calculations are given in the Appendix.

may provide the only feasible, unambiguous relative test of the two models. The analyses described in the next section indicate that such a clear cut test can be made.

III. DEPENDENCE OF CONDITIONING ("INACTIVATION") CURVES ON TEST VOLTAGE

The peak sodium conductance, g_p, is defined in terms of the peak sodium current, I_p, and the sodium ion driving force, $(E_m - E_{Na})$, where E_m is the clamped membrane potential and E_{Na} is the sodium equilibrium emf. Thus

$$g_p = I_p/(E_m - E_{Na}).$$

Using this operational definition, it has been found experimentally that the magnitude of g_p depends both on the membrane potential from which the test clamp starts and the potential of the test clamp. Two types of experimental results are

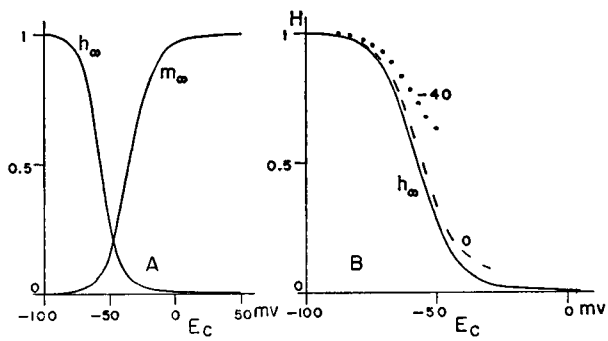

FIGURE 4 (*A*) Equilibrium values of the I-HH parameters m and h. (*B*) Comparison of h_∞ (solid) and predicted conditioning curves at test potentials of 0 (dashed) and −40 mv (dotted). The latter curves were computed under the assumption that $\tau_m = \tau_h$.

often presented. Either, (*a*) the holding potential is held at a fixed value and the dependence of g_p on the test clamp is determined, or (*b*) the test clamp potential is held at a fixed value and the dependence of g_p on the holding (or conditioning) potential is determined. For both types of experiments it is customary to present *relative* values of g_p, referred to the maximum g_p attained in the given experiment. Thus all g_p values in (*a*) are divided by the value of g_p obtained at large depolarizing test voltages, while in (*b*) they are divided by the value of g_p obtained at large hyperpolarizing conditioning voltages. Commonly only one conditioning voltage is used in (*a*) and only one test voltage in (*b*), the implication being that such relative curves are *invariant* with respect to the fixed conditioning or test voltage. The degree to which the I-HH and II-H model fibers on the one hand, and the experimental nerve fiber on the other, show the presence or absence of such invariances will be discussed in this section. The primary emphasis will be on the conditioning curves of case *b* since peak current ratios at a fixed test potential lead directly to g_p ratios,

the $(E_m - E_{Na})$ factor cancelling out. For case *a* the value of E_{Na} is required before experimental g_p ratios can be calculated and a greater experimental uncertainty is thus introduced.

I-HH

We consider first the predictions of the I-HH model for the simple conditioning experiment in which one determines the effect on the peak sodium current of preceding, long-lasting, conditioning prepulses. The test potential, E_T, is maintained at some fixed value and the voltage of the conditioning preclamp, E_C, is varied over both hyperpolarizing and depolarizing values. According to the HH model, the resulting peak sodium currents should be approximately proportional to the magnitude of h at the start of the test clamp, and therefore to the equilibrium values of h, h_∞, reached during the preclamp. The ratios of the peak current to that obtained after a very large hyperpolarizing preclamp, when h_∞ attains its maximum value of unity, should therefore closely follow the h_∞ curve, shown by the solid curve in Fig. 4*B*. A precise application of the HH equations shows that small departures of the experimental points from the invariant h_∞ curve are predicted for some ranges of test and conditioning voltages. Since it is just such departures that turn out to be important when a comparative test of the models is made, they are analyzed below.

Equations 1–3 of Fig. 1 may be rewritten as

$$g = m^3 h \tag{6}$$

$$\dot{m} = -(m - m_e)/\tau_m \tag{7}$$

$$\dot{h} = -(h - h_e)/\tau_h \tag{8}$$

where g is expressed in units of $\bar{g}$ and the α and β parameters have been rewritten in terms of equilibrium values (m_e, h_e) and time constants (τ_m, τ_h). The solutions to equations 7 and 8 may be written

$$m = m_e + (m_\infty - m_e) \exp -t/\tau_m \tag{9}$$

$$h = h_e + (h_\infty - h_e) \exp -t/\tau_h \tag{10}$$

where h_∞ and m_∞ are the values at the start of the test clamp, and are thus the equilibrium values at the long-lasting conditioning voltage, while h_e and m_e are the equilibrium values for the test clamp. The dependence of these equilibrium values on the membrane potential for a fiber obeying the original 1952 HH equations is shown in Fig. 4*A*. The resting potential is arbitrarily taken to be −60 mv.

The maximum value of g, g_p, is obtained when $\dot{g} = 0$, a condition that may be rewritten, using equations 6–8, as

$$3(m_e - m_p)/m_p\tau_m = (h_p - h_e)/h_p\tau_h, \tag{11}$$

where m_p and h_p are the values of these variables at the conductance maximum. A second equation relating m_p and h_p may be obtained by eliminating the time, t, between equations 9 and 10, namely

$$[(m_e - m_p)/(m_e - m_\infty)]^{\tau_m} = [(h_p - h_e)/(h_\infty - h_e)]^{\tau_h}. \tag{12}$$

In principle equations 11 and 12 may be solved simultaneously for m_p and h_p in terms of their initial (m_∞, h_∞) and final (m_e, h_e) values and the time constants (τ_m, τ_h) appropriate to the test voltage. In practice the equations must be solved by a numerical method rather than an analytical one. In order to obtain insight into the expected behavior we first consider several special cases. Throughout we assume a 6°C, unperfused fiber characterized by the 1952 HH equations, with an absolute resting potential of −60 mv.

$h_e \ll h_\infty$, h_p. This approximation should be valid for test potentials greater than −30 mv, and conditioning potentials less than −60 mv. Under these conditions one may set $h_e = 0$ in equation 12. With this simplification a solution may be obtained in closed form, namely

$$m_p = m_e 3\tau_h/(\tau_m + 3\tau_h) \tag{13}$$

$$h_p = h_\infty[m_e\tau_m/(m_e - m_\infty)(\tau_m + 3\tau_h)]^{\tau_m/\tau_h}. \tag{14}$$

For a given test potential, the ratio of peak sodium conductance at one conditioning potential to that obtained at a very hyperpolarizing conditioning potential ($h_\infty = 1$, $m_\infty = 0$) shall be designated by H. From equations 13 and 14 we then obtain

$$H = h_\infty/[1 - (m_\infty/m_e)]^{\tau_m/\tau_h}. \tag{15}$$

The quantities m_e, τ_m, and τ_h are constants fixed by the test clamp used, while h_∞ and m_∞ are dependent on the particular conditioning potential used. For large hyperpolarizing conditioning voltages m_∞ will be negligible compared to m_e and equation 15 reduces to $H = h_\infty$. As the conditioning voltage is made progressively less hyperpolarizing, m_∞ increases and the denominator of equation 15 becomes smaller. H thus becomes larger than h_∞, as shown in the dashed curve of Fig. 4*B*. This departure of the H curve from the h_∞ curve becomes more prominent at smaller test voltages where m_e is smaller (dotted curve of Fig. 4*B*).

It should be noted that H is an experimentally observable quantity, operationally defined as the ratio of peak sodium current obtained at a given conditioning potential to the peak current obtained when a very hyperpolarizing potential is used. The right-hand side of equation 15 is then a statement of the prediction of the I-HH model under the restrictions of the assumed approximations.

$\tau_m = \tau_h$. As the conditioning voltage is made less hyperpolarizing, departures of H from h_∞ are to be expected not only from the breakdown of the

approximation $(m_\infty/m_e) \ll 1$, but also from a breakdown of the initial assumptions leading to equation 15, i.e. $h_e \ll h_\infty$, h_p. The effect of the breakdown of this latter condition should also appear earlier and be more serious at low test voltages. By choosing the special case, $\tau_m = \tau_h$, for which a solution of equations 11 and 12 in closed form is possible, the qualitative nature of both these effects may be investigated.

Letting $\tau_m = \tau_h$, but making no other assumptions or approximations, one obtains

$$h_p = (m_e h_\infty - m_\infty h_e)/4(m_e - m_\infty) \tag{16}$$

$$m_p = 3(m_e h_\infty - m_\infty h_e)/4(h_\infty - h_e). \tag{17}$$

The qualitative aspects of H become particularly clear if the additional assumption is made that (m_∞/m_e), (h_e/h_∞) and (h_e) are small compared to unity (but not completely negligible). Under these conditions the H ratio is given by

$$H = h_\infty[1 + (m_\infty/m_e) + 3(h_e/h_\infty) - 3h_e]. \tag{18}$$

It is apparent that as the conditioning voltage is made less hyperpolarizing the resulting increase in m_∞ and decrease in h_∞ cause both (m_∞/m_e) and (h_e/h_∞) to increase. The H curve will therefore again depart from the h_∞ curve, as shown by the dashed curve in Fig. 4*B*. For a less depolarizing test potential, m_e is smaller and h_e is larger, and the departures appear earlier and are more prominent (dotted curve).

General Case. Although equation 18 was derived on the assumption that $\tau_h = \tau_m$, the qualitative nature of the departure of H from h_∞ will be the same even if this restriction is removed. However, if the ratio (τ_m/τ_h) is much less than unity the departures of H will be correspondingly smaller. For the original HH fiber, where the ratio (τ_m/τ_h) is considerably less than unity over all voltage ranges of interest, numerical solutions of equations 11 and 12 lead to the curves shown in Fig. 5. The solid curve shows the dependence of h_∞ on the conditioning potential.

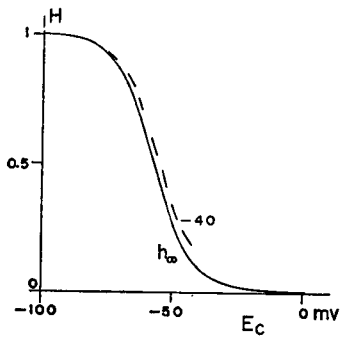

FIGURE 5 Predictions of the 1952 HH equations, assuming a resting potential of −60 mv. Solid curve, equilibrium values of h. Dashed curve, predicted conditioning curve for a test potential of −40 mv.

Test potentials greater than -10 mv lead to departure of H from the h_∞ curve too small to be plotted in Fig. 5. The dashed curve shows the dependence of H on conditioning voltage for a very small test voltage ($E_T = -40$ mv). The departures are thus similar to those shown in Fig. 4*B*, but much smaller in magnitude. Since the absolute magnitudes of the conductances become smaller as the test potential is made less depolarizing, the corresponding shift of conditioning curves to the right (dashed curve) might be very difficult to detect experimentally.

We may conclude from the above discussion that a "normal", 1963, HH fiber should lead to a conditioning H curve that is essentially independent of the test potential used and follows very closely the h_∞ curve. Under some circumstances, small departures of H from h_∞ might become observable. In the latter case these departures will be such that the H curve will be shifted in the depolarizing direction

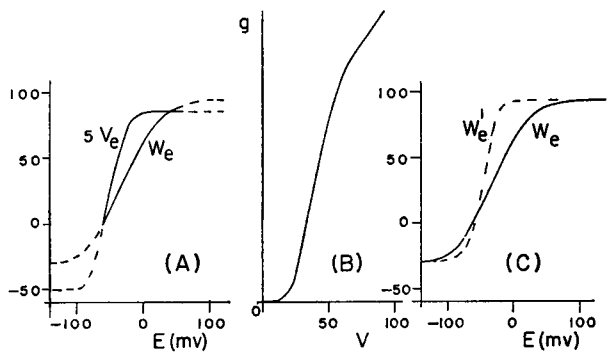

FIGURE 6 Parameters of the II-H model. (*A*) Equilibrium values of v and w as a function of membrane potential (dashed portions represent extrapolations from the 1963 analysis). (*B*) Dependence of the sodium conductance on the instantaneous value of v. (*C*) Solid curve, w_e values used in Fig. 8*A*, dashed curve, w_e' values used in Fig. 8*B*.

as the test voltage is made less depolarizing, i.e. shifted *opposite* to the change in test voltage.

II-H

Before entering upon a quantitative discussion of the predictions of the Hoyt example of a class II model, as specifically applied to conditioning curves, some relative aspects of the behavior of experimental fibers and the I-HH and II-H models are worth noting. Except under unusual circumstances (6, 7) the early increase of conductance under a depolarizing clamp is transient in nature; the resting conductance of the early (sodium) channel is very small at all values of the membrane potential. In the I-HH model this small resting conductance results from the fact that, as shown in Fig. 4*A*, at all potential values the equilibrium values of either m or h are very small, so that the equilibrium value of the product (hm^3) always remains small. On the other hand, in the II-H model the equilibrium values of v always remain below the level at which the function $g(v)$ becomes very appreciable (Fig. 6). The

normal transient response under a depolarizing clamp, characterized in the experimental fiber by a rapid rise in conductance followed by a somewhat slower fall, is obtained in the I-HH model by a rapid increase in m accompanied by a slower, independent decrease in h. In the II-H model, as noted in connection with Fig. 3, the variable v at first follows the rapid rise in w. Since the change in equilibrium value of w is much greater than that of v, v undergoes a large overshoot before returning more slowly to its new equilibrium.

The effect of changes in the conditioning potential on the response of the II-H model to a fixed test clamp is illustrated in Fig. 7. The initial rise in v is determined by the change in w (first term in equation 5), not by the absolute magnitude of w. The curves labeled 2 correspond to a more depolarizing conditioning voltage than those labeled 1. As a result w starts in curve 2 from a value, $w_{\infty 2}$, closer to its final equilibrium than its starting point in curve 1, $w_{\infty 1}$. The peak change in v is therefore much less in curve 2 than in curve 1. The dashed curves show the course that v

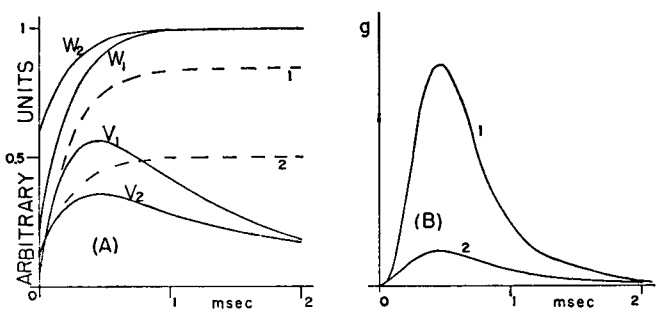

FIGURE 7 Conditioning effect in the II-H model. (*A*) Time dependences of v and w for two different initial (conditioning) potentials, but the same clamping (final) potentials. The dashed curves show the time courses that v would follow in the absence of coupling to w. (*B*) Time dependences of the conductance for the two conditioning potentials of *A*.

would take if the second term in equation 5 were not present, identical to the course that w takes except displaced vertically. The corresponding changes in g are also shown, and are obtained by applying the functional transformation of Fig. 6*B* to the $v(t)$ curves. The magnitude of the peak sodium conductance is seen to be reduced at the more hyperpolarizing conditioning potential.

Quantitative prediction of the shape of a conditioning curve and the dependence of this shape on the test potential used can be obtained by a method similar to that used for the I-HH model. The solutions to the coupled equations 4 and 5 may be written

$$w = w_e - (w_e - w_\infty) \exp(-k_1 t) \tag{19}$$

$$v = v_e - [(w_e - w_\infty)k_1/(k_1 - k_3)] \exp(-k_1 t) + [(v_\infty - v_e) + (w_e - w_\infty)k_1/(k_1 - k_3)] \exp(-k_3 t), \tag{20}$$

where (v_e, w_e) and (v_∞, w_∞) are the equilibrium values at the test and conditioning potentials respectively. The peak value of g, g_p, is obtained when v reaches its peak value, v_p, and this occurs when $\dot{v} = 0$. This condition may be rewritten

$$k_3(v_p - v_e) = k_1(w_e - w_p) \tag{21}$$

where w_p is the value of w at the moment when v reaches its peak value, v_p. Equations 19–21 may be used to eliminate both the time to reach peak and w_p. Since the resulting equation is somewhat cumbersome, it is convenient in the present discussion to use the simplification afforded by the approximation

$$(v_e - v_\infty) \ll (w_e - w_\infty), \tag{22}$$

which is often valid. Under these conditions one obtains

$$v_p - v_e = (w_e - w_\infty)[k_3/k_1]^{k_3/(k_1-k_3)}. \tag{23}$$

This analytic expression confirms the earlier conclusion that it is the *difference* between the initial and final values of w that primarily determines the magnitude of the peak value of v which in turn determines the peak value of the conductance. As a result of this dependence on a difference, the shape of conditioning curves will be very dependent on the test potential used. However, if the value of w_e saturates at large depolarizing test potentials, as shown in Fig. 6*A*, a limiting curve should result at these large test potentials. In this respect the two models are similar in their prediction. A striking qualitative difference appears, though, when one compares the way in which divergences from the limiting curves appear at less depolarizing test potentials. A given change in w_∞ will cause a larger fractional change in the difference term of equation 23 when w_e is small (small depolarizing test potential) than when w_e is large (large depolarizing test potential). The relative conditioning curves will

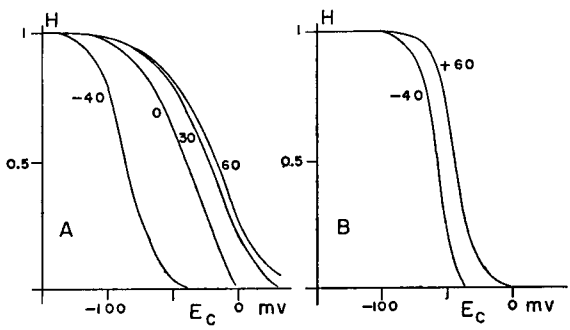

FIGURE 8 Conditioning curves predicted by the Hoyt model. For curves *A* the 1963 parameters of Fig. 6*A* and *B* were used. For curves *B* the steepened w_e' curve of Fig. 6*C* was used. The numbers accompanying each curve indicate the test voltage in millivolts.

therefore tend to be shifted in the hyperpolarizing direction as the test potential is made less depolarizing (Fig. 8*A*). Comparison of Fig. 8 with Figs. 4 and 5 shows that the shifts predicted by the two models are *opposite* in direction.

The conditioning curves of Fig. 8*A* were calculated using equations 19–21 in which no approximations have been made. The values of v_e, v_∞, w_e, w_∞, and $g(v)$ were taken from the curves of Figs. 6*A* and 6*B*. The solid portions of the curves of Fig. 6*A* represent the values originally chosen to fit the data from the HH fiber ✱17 (3), while the dashed portions represent reasonable extrapolations. Tabular values are given in the Appendix. If the dependence of w_e on potential is steepened, as shown in Fig. 6*C*, the magnitudes of the shifts in the conditioning curves are reduced, but their direction remains the same, Fig. 8*B*.

Comparison with Experiment

It should be possible to compare the behavior of experimental fibers with the contrasting predictions of the I-HH (Fig. 5) and the II-H (Fig. 8) models. Unfortunately the evidence existing in the published literature is meager; most authors present conditioning curves obtained at only one test potential and the value of that test potential is often not stated. The evidence that has been found is presented below.

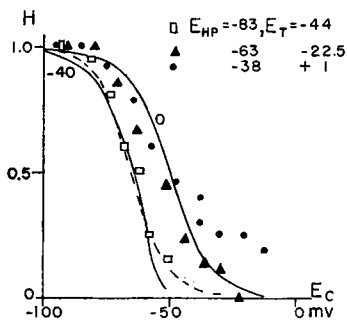

FIGURE 9 Comparison of experimental conditioning curves with the predictions of I-HH and II-H. Experimental points from Adelman and Fok (8); external solution, ASW; internal perfusate, 33 mM K. Dashed curve: the I-HH curve for h_∞. Solid curves: prediction of the II-H model for test potentials 0 and −40 mv.

In Fig. 9 we show the results of a series of conditioning experiments reported by Adelman and Fok (8) on a perfused squid axon. The external and internal solutions were respectively ASW and 33 mM K (K_2SO_4, KH_2PO_4, K_2PO_4, and sucrose). Three different holding potentials were used, and for each holding potential a different test potential was chosen. (The different test potentials were chosen so that the peak sodium current was close to its maximum for that holding potential.) Long-lasting conditioning prepulses were then applied to the fiber, and the peak sodium current during the second, test, pulse was measured. According to both the I-HH and the II-H models, there should be no distinction between holding at some potential and prepulsing for a long time to that potential. However, the divergences of the experimental conditioning (H) curves from a single invariant curve (h_∞) led Adelman and Fok to postulate the existence of an additional, very long time constant, inactivation effect dependent on the holding potential. No such additional effect due to the

holding potential need be introduced if the II-H model is used. Rather, the differences between the experimental H curves can be completely accounted for by the differences in the test potentials used. The predictions of the II-H model for test potentials of 0 and -40 mv are shown by solid curves while the dashed curve shows the I-HH h_∞ curve of Fig. 5. For the solid curves the steepened w_e curve of Fig. 6*C* was used. All three theoretical curves have been shifted to the left by the identical amount of 8 mv. The experimental observation of such a shift at low internal ionic strength has been reported before (5), and is distinct from the relative shifts caused by changes in the holding potential that are under consideration here. It is obvious that the direction and magnitude of the latter shifts with holding potential predicted by II-H are in good agreement with the experimental results of Fig. 9. On the other hand, comparison with Figs. 4 and 5 shows that the I-HH predictions are in disagreement with the results of Fig. 9, both as to the magnitude and, more importantly, the direction of the shift accompanying changes in test potential.

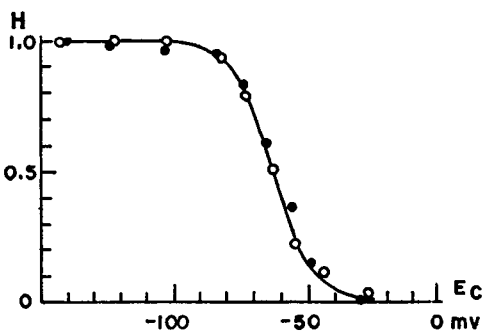

FIGURE 10 Conditioning curves obtained by Chandler and Meves (9). Internal perfusate: 300 mM KCl; external solution: ASW. Filled circles: using early outward (K) currents, test potential of +97 mv. Open circles: using early inward (Na) currents, test potential of -11 mv.

Unlike the Adelman and Fok results shown in Fig. 9, Chandler and Meves (9) have reported an experiment in which no shift of the conditioning curve with test potential was observed. The Chandler and Meves results, obtained on a squid axon perfused with 300 mM KCl and with ASW as the external medium, are shown in Fig. 10. Two conditioning curves were run, one using peak, early, inward (sodium) currents at a test potential of -11 mv, and the other using peak, early, outward (potassium) currents at a test potential of +97 mv. The overlap of the two conditioning curves is obviously in agreement with the prediction of I-HH. However, this overlap is also not at variance with the predictions of II-H. As shown earlier in Fig. 8, this latter model predicts that no appreciable shifts of the conditioning curves will occur so long as the test potential is kept sufficiently depolarizing, (greater than -20 mv under normal ionic conditions). One may conclude that the results of Fig. 10 are in agreement with both models.

While conditioning experiments may afford the clearest way of testing the relative merits of the two models, lack of published results, other than the two quoted above, has led to a further search for ways to make this experimental test. The peak con-

ductance is obviously dependent on two potentials, that of the test clamp, E_T, and that of the conditioning clamp, E_C, i.e.

$$g_p = g_p(E_T, E_C).$$

Analogous to the dependence of the plate current of triodes on both grid and plate voltages, two types of "characteristic curves" may be used to describe g_p. Either E_T may be held at different fixed values and E_C varied, or E_C may be held at different fixed values and E_T varied. The former correspond to Fig. 9. No published examples of the latter, which present two or more curves of g_p vs. E_T at different E_C's, have been found. However, two published examples have been found of the related, more basic, curves of peak currents vs. E_T, obtained at two or more different values of E_C. These are presented in Fig. 11 together with sample curves from the two models.

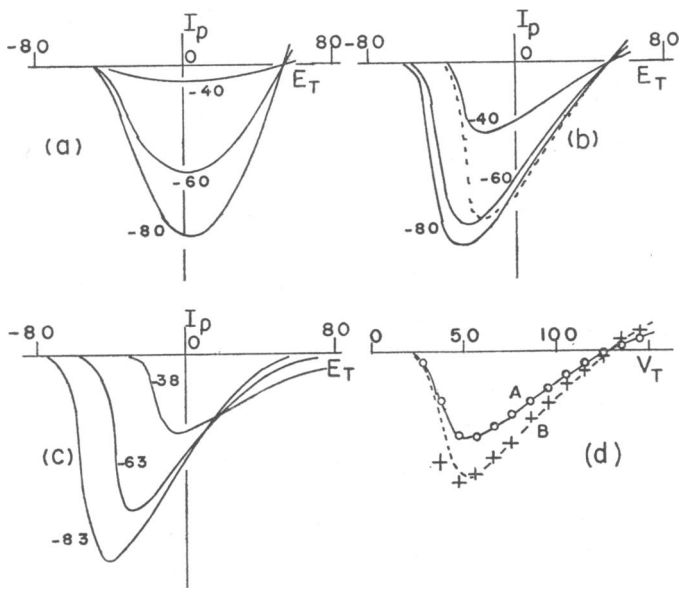

FIGURE 11 Peak early currents. Predictions of the I-HH model, curves *a*, and the II-H model, curves *b*, for holding potentials of −80, −60, and −40 mv. Dashed curve in (*b*) was obtained by multiplying the −40 mv curve by 2.2. Curves *c*: experimental results of Adelman and Fok (8) for the same fiber and solutions as in Fig. 9. Curves *d*: experimental results of Frankenhaueser (10) on a *Xenopus* node; test voltages (abscissa) are given relative to the resting potential. For the circles and curve *A* the holding potential was the resting potential. For the crosses the holding potential was −19 mv (hyperpolarization) relative to the resting potential. Dashed curve *B* is curve *A* multiplied by 1.44.

The theoretical curves of Fig. 11*a* and *b* were calculated assuming that the absolute resting potential for the I-HH and II-H models is −60 mv, and further assuming an absolute value of +55 mv for the sodium emf. For the I-HH model, all three peak

current curves shown in (*a*) are essentially identical except for constant multiplicative factors that relate the three curves to each other. This behavior follows from the fact that the conditioning curves of Fig. 5 are essentially identical, independent of E_T. The multiplicative constants relating the curves of Fig. 11*a* are merely the ratios of the H values in Fig. 5 for conditioning potentials of -80, -60, and -40 mv.

The II-H curves of Fig. 11*b* show a quite different behavior. As a result of the dependence of the conditioning curves of Fig. 8 on test potential, the peak current curves are not related by fixed multiplicative constants. For example, multiplication of curve 1 by 2.2 yields the dashed curve, in good agreement with curve 3 for test potentials greater than -10 mv, but in serious disagreement for test potentials less than -10 mv. In this model the positioning of the peak current maxima and the shapes of the curves are obviously dependent on the conditioning (holding) potential used.

In Fig. 11*c* we show the peak current curves obtained by Adelman and Fok on the same fiber and under the same perfusion conditions as that shown in Fig. 9. Qualitatively these results are in good agreement with the II-H curves. The quantitative discrepancies can in part be explained by the shift caused by the low ionic strength of the internal perfusate and by the fact that no sodium was present internally. The latter fact undoubtedly distorts the shape of the curves at high depolarizations. In Fig. 11*d* we show results obtained by Frankenhaeuser (10) using a *Xenopus* node. Test voltages are here measured relative to the normal resting potential. The circles and curve A were obtained for a holding potential at the resting potential. The crosses were obtained for a holding potential of -19 mv (hyperpolarization) relative to the resting potential. The dashed curve B, was obtained by multiplying A by 1.44. From the agreement between curve B and the experimental crosses for large depolarizing test voltages, Frankenhaeuser concludes that inactivation is independent of test potential, as predicted by the I-HH model. The disagreement for small test voltages might, on the other hand, equally well be used to support the II-H model.

IV. DISCUSSION

From the results presented in the preceding sections it is clear that while many clamp experiments may be incapable of distinguishing between the two models analyzed, so called inactivation curves (here called conditioning curves), obtained with more than one test potential should be able to perform this function. Alternatively, peak current curves obtained at more than one conditioning potential might often serve the same purpose. It is worth noting that sodium ions should be present in the internal perfusate, in sufficient amount to enable an unambiguous sodium emf to be operationally defined, and to avoid the obvious nonlinearities present in Fig. 11*c* at large depolarizations.

It is unfortunate that there exists in the literature such a paucity of experimental results of the appropriate nature. The limited experimental results analyzed in the

preceding section strongly suggest that the predictions of the II-H model are in better agreement with these results than those of the I-H model. A more definite conclusion must await the analysis of additional experiments.[4]

The question remains as to the extent to which the predictions of the I-HH and the II-H models are specific to these two models or are characteristic, at least qualitatively, of other possible models of their respective classes. In the following discussion no attempt is made at generality. Rather, a few additional examples from each class will be considered.

Turning first to class I models, the only ones to be considered here are similar to HH in that they contain just two independent variables, each obeying first order linear kinetics (exponential time dependences). We thus assume

$$g_N = f_1(m)f_2(h) \tag{24}$$

where

$$\dot{m} = -(m - m_e)/\tau_m \quad \text{and} \quad \dot{h} = -(h - h_e)/\tau_h .$$

Both f_1 and f_2 are assumed to be monotonically increasing functions of m and h, respectively. In order that the conductance under a depolarizing clamp first increase and later decrease with time it is further necessary that the equilibrium values m_e and h_e be monotonically increasing and decreasing functions, respectively, of the membrane potential. Within these restrictions modifications of two types may be made. First, variations may be made in: the steepness of each of the two equilibrium curves, $m_e(E_m)$ and $h_e(E_m)$; in the relative positions of these equilibrium curves along the voltage axis; and in the relative value of the two time constants. From the earlier discussion it should be obvious that the dependence of conditioning curves on test potential will be affected only in degree, not in qualitative character, by such modifications, and should therefore be similar to that shown in Fig. 5. It is modifications of this nature that Noble (11) found to be necessary when he adapted the HH model to the behavior of cardiac muscle. Unfortunately Noble reports no experiments that can be used to test the predicted behavior.

The second type of modification consists of variations of the two monotonic functions, $f_1(m)$ and $f_2(h)$. One simple subclass consists of power law functions,

$$g = m^r h^s, \tag{25}$$

where r and s are positive constants. The only change that this generalization makes in the earlier treatment is to substitute the number $p = r/s$ for the number 3 appearing in equation 11. It is obvious that the qualitative form of the results of con-

[4] It is hoped that the analysis of experiments conducted at Woods Hole by Dr. William J. Adelman, Jr. and coworkers during the summer of 1967 will, in part, serve this purpose.

ditioning experiments will be unaffected by this change. The change from (m^3h) to (m^2h) that Frankenhaeuser (12) found necessary to account for the early sodium currents of the myelinated fibers of *Xenopus* should therefore again lead to the prediction of Fig. 5. For the reason discussed in relation to Fig. 11*d* (the coincidence of the crosses with the falling portion of the dashed curve) no experimental test of this prediction was made by Frankenhaeuser.

In addition to the simple power law functions of equation 25, of which the choices of HH, Noble, and Frankenhaeuser are examples, other biological preparations or other experimental conditions may require other functions for the best fit to the early current vs. time curves under a voltage clamp. No attempt will be made here to anticipate all possible future choices for these functions. It is, though, worth noting that in addition to power law functions, some simple algebraic functions such as $f(x) = 2x^3/(1 + x)$ and $f(x) = (ax + bx^2)$, where a and b are both positive, should lead to current curves of qualitatively the correct shape (here x stands for m or h). Further, simple mathematical tests show that the use of either of these specific functions for $f_1(m)$, or $f_2(h)$, will again lead to conditioning curves whose dependence on test voltage is qualitatively similar to that shown for the I-HH model in Figs. 4 and 5.

Turning to class II models, we shall only consider the case of two coupled equations, linear and first order. The most generalized form for this case is

$$\dot{w} = -k_1(w - w_e) - k_2(v - v_e) \tag{26}$$

$$\dot{v} = -k_4(w - w_e) - k_3(v - v_e) \tag{27}$$

These equations differ from equations 4 and 5 only in that a coupling term has been added in equation 26, and k_4 replaces k_1 in equation 27. Assuming as earlier that $(v_e - v_\infty) \ll (w_e - w_\infty)$, solution of these equations for the peak value, v_p, yields

$$v_p - v_e = K(w_e - w_\infty) \tag{28}$$

where K is a function of the four k's. Comparison of equation 28 with equation 23 shows that the two are identical in form. If to equations 26 and 27 we add the hypothesis that the sodium conductance is a monotonic function of v, i.e. $g = g(v)$, the resulting class II model will show the same qualitative behavior as II-H, and, in particular, the dependence of conditioning curves on test potential will be as shown in Fig. 8.

The kinetic equations for the configurational changes of the Goldman (4) model can be put into the form of equations 26 and 27. Exact correspondence can then be obtained between v and the concentration of sodium binding configurations, n_{II}, and between $-w$ and the total concentration of calcium binding configurations, n_I. The four k constants of equations 26 and 27 are then functions of the twelve

Goldman constants (six k's, p, q, q', M, k_e and K'). If one then assumes that the sodium conductance depends in a monotonic fashion on the concentration n_{II}, exact correspondence will result between this model and those considered earlier. However, rather than a linear, ohmic, relation between instantaneous current and driving voltage implicit in the use of conductances, Goldman assumes that, for a given instantaneous n_{II}, nonlinear processes control the current. This is analogous to the use by Frankenhaeuser of permeabilities rather than conductances. Although

TABLE I

1963 PARAMETER VALUES (6.5°C)

$V = E - E_R$	k_1	k_2	v_e	w_e	E ($E_R = -60$ mv)
mv	$msec^{-1}$	$msec^{-1}$			*mv*
$-\infty$			−10.0	−30.0	$-\infty$
−70			−10.0	−29.8	−130
−60			−10.0	−29.1	−120
−50			−10.0	−27.8	−110
−40			−10.0	−25.6	−100
−30			−9.8	−22.3	−90
−20			−8.1	−17.2	−80
−10			−4.4	−9.7	−70
0	5.40	0.111	0.0	0.0	−60
10	3.82	0.091	4.4	10.4	−50
20	2.97	0.124	8.7	21.1	−40
30	2.75	0.199	12.5	31.8	−30
40	3.64	0.314	15.1	42.5	−20
50	4.19	0.470	16.3	53.0	−10
60	4.43	0.655	16.8	62.4	0
70	4.53	0.847	17.0	70.2	10
80	4.61	1.05	17.0	76.4	20
90	4.67	1.25	17.0	81.7	30
100	4.72	1.45	17.0	85.5	40
110	4.75	1.65	17.0	88.1	50
120	4.77	1.85	17.0	89.8	60
130	4.78	2.05	17.0	91.0	70
140	4.79	2.25	17.0	91.7	80
$+\infty$			17.0	93.0	$+\infty$

the behavior may be changed quantitatively by such nonlinearities, the qualitative nature should be unchanged, since it is determined by the kinetic equations (equations 26 and 27).

In summary: All those class I models analyzed show the behavior of Figs. 4 and 5; conditioning curves are shifted in the depolarizing direction as the test potential is made less depolarizing, but these shifts may often be too small to detect. All those class II models analyzed show the behavior of Fig. 8; conditioning curves are shifted

in the hyperpolarizing direction as the test potential is made less depolarizing, but these shifts only occur over a *limited* range of test potentials.

APPENDIX

Calculations Using the Hoyt Model

As originally developed (3), the Hoyt example of a class II model, diagrammed at the right of Fig. 1, was fitted to the clamp conductance data of axon #17 as given by HH (1) in their Fig. 6. Conductance data from only the one fiber was used. Inspection of Figs. 7 and 9 of HH (1) reveals that their axon #17 was not a completely typical one. For this reason the values of the parameters of the Hoyt model are far from certain and no attempt has therefore been made to fit by analytic equations the k vs. voltage curves so obtained. All calculations using this model have been made from tabular data. Coarse data for the four parameters are given in Table I. In actual calculations, tabular values to the nearest millivolt have been used. Linear interpolation, to fractions of a millivolt, has been used in digital computation of action potentials. The voltage scale at the left in Table I is that relative to the resting potential of the HH #17 axon. The voltage scale at the right gives an approximate absolute scale, assuming a resting potential of −60 mv. This absolute voltage scale, which may be incorrect by as much as 5 mv, is what has been used for the calculations given in Figs. 2, 8, 9, and 11. The four parameter values given in the table are those for a temperature of 6–7°C. They may be scaled to other temperatures using a Q_{10} of 3.

TABLE II

g_N VALUES FOR AXON #17

v	g_N
	mmho/cm²
−5	0.0000
0	0.0006
5	0.038
10	0.122
15	0.390
20	1.03
25	2.50
30	5.26
35	8.15
40	11.05
45	13.88
50	16.45
55	18.87
60	21.08
65	22.30
70	23.3
75	24.3
80	25.3
85	26.3

Tabular values have also been used for the $g_N(v)$ functional dependence. Coarse values of this dependence, as fitted to axon #17, are given in Table II. In actual calculations, tabular values to the nearest 0.5 value of v are used, with linear interpolation performed in between

these values of v. The tabular values of Table II are given in the mmho/cm^2 values appropriate to the HH axon #17. Adjustment to the appropriate values for other fibers is made by choice of a simple, multiplicative scaling factor.

For a voltage clamp situation the two coupled equations of Fig. 1, equations 4 and 5, can be solved for the v dependence separately, yielding the second order v equation

$$\ddot{v} + (k_1 + k_3)\dot{v} + k_1k_3(v - v_e) = 0, \tag{A1}$$

and the w equation given earlier

$$\dot{w} = -k_1(w - w_e). \tag{A2}$$

The solution to equation A1 is

$$v = C_1 + C_2 \exp(-k_1t) + C_3 \exp(-k_3t), \tag{A3}$$

TABLE III

STEADY-STATE CONDITIONING—SAMPLE ANALYSIS, 6.5°C

	$E_C = -60$ mv, $w_0 = 0.00$, $v_0 = 0.00$		$E_C = -40$ mv, $w_0 = 21.1$, $v_0 = 8.7$	
	$E_T = -30$ mv	$E_T = +10$ mv	$E_T = -30$ mv	$E_T = +10$ mv
k_1	2.75 msec^{-1}	4.53 msec^{-1}	2.75 msec^{-1}	4.53 msec^{-1}
k_3	0.199 msec^{-1}	0.847 msec^{-1}	0.199 msec^{-1}	0.847 msec^{-1}
v_e	12.5	17.0	12.5	17.0
w_e	31.8	70.2	31.8	70.2
C_1	12.5	17.0	12.5	17.0
C_2	−34.3	−86.7	−11.5	−52.9
C_3	21.8	69.7	7.7	44.6
v_p	28.4	53.7	18.4	40.7
g_p	4.36 mmho/cm^2	18.25 mmho/cm^2	0.85 mmho/cm^2	11.46 mmho/cm^2

where the coefficients are given by

$$C_1 = v_e \tag{A4}$$

$$C_2 = -(w_e - w_0)/[1 - (k_3/k_1)] \tag{A5}$$

$$C_3 = (v_0 - v_e) - C_2\,. \tag{A6}$$

The solution to equation A2 is

$$w = w_e - (w_e - w_0) \exp(-k_1t). \tag{A7}$$

In the above equations w_0 and v_0 are the values of these variables at the start of the clamp, while w_e and v_e are the equilibrium values for the given clamping voltage.

Sample Calculation of Steady-State Conditioning (Inactivation) Curves

For a given test potential E_T, the values of k_1, k_2, v_e, w_e are fixed in equations A3–A6. The effect of a conditioning prepulse on the time course of v, and therefore of $g_N(v)$, occurs through

the effect of the preclamp on w_0 and v_0. In Table III sample calculations of the coefficients C_1, C_2, and C_3 are given for two test (-30 mv and $+10$ mv) and two conditioning (-40 mv and -60 mv) potentials, using the 6.5°C values given in Table I. The results of application of equation A3 then lead to the tabulated peak values of v, v_p, while use of Table II leads to the associated peak conductance values, g_p, in the conductance scale of HH axon #17.

It is apparent from the results presented in Table III that there is no single quantity analogous to the HH "inactivation" variable h to which, in the Hoyt Model, one may ascribe the conditioning effect. For a given test potential, the peak conductance is indeed smaller at $E_C = -40$ mv than at $E_C = -60$ mv, but the fractional size of this reduction is obviously very dependent on the test potential used.

The Two Pulse Experiment of Fig. 2

In order to fit the Hoyt model to the Chandler, Hodgkin, and Meves experiment of Fig. 2 the parameters k_1 and k_3 of Table I must first be scaled from 6.5°C to 0°C. No temperature scaling should be required for the equilibrium values, w_e and v_e. Using a Q_{10} of 3, one then obtains from Table I the appropriate values for a resting potential of -60 mv and a test

TABLE IV

DOUBLE PULSE EXPERIMENT

	Parameter values for 0°C		Parameter values chosen	
	-60 mv	$+10$ mv	-60 mv	$+10$ mv
k_1	2.7 msec^{-1}	2.26 msec^{-1}	0.6 msec^{-1}	2.0 msec^{-1}
k_3	0.055 msec^{-1}	0.424 msec^{-1}	0.06 msec^{-1}	0.13 msec^{-1}
v_e	0.0	17.0	0.0	19.2
w_e	0.0	60.2	0.0	60.0

potential of $+10$ mv, as shown at the left in Table IV. Only minor adjustments were required for most of the parameters. However, in order to obtain a close fit to the experimental points major adjustments were required for k_1 (-60) and k_3 ($+10$). As mentioned in section II, a similar major adjustment was found necessary in fitting the HH model to the same experimental data. The final values chosen are shown at the right in Table IV.

Using the parameters at the right of Table IV one may compute the appropriate values of C_1, C_2, C_3, w_0, and w_e for the first depolarization, as in the preceding section. Equations A3 and A7 may then be used to determine the time course of v and w during the first depolarization. The values $w(t_1)$ and $v(t_1)$ are then used as initial values for the repolarization period, and new C_1, C_2, and C_3 values are computed. Equations A3 and A7 are then used again to determine w and v values at the end of the 7.7 msec repolarization period. Finally, these are used as initial values to determine the third set of C_1, C_2, and C_3 values from which the time course of v during the second depolarization period is obtained. The maximum value of v attained during the second depolarization is then determined and the corresponding maximum value of g_N is obtained from Table II. In this way the dashed curve in the lower half of Fig. 2 is traced out.

As can be seen from the foregoing description, the qualitative nature of the dependence of the peak sodium conductance during the second pulse on the duration of the first pulse is very dependent on the parameter values at the holding and test potentials, and on the duration of the repolarization period. The Chandler, Hodgkin, and Meves statement for this model,

that the "inactivation rate during the first pulse is proportional to the conductance," is obviously not true in general.

The author wishes to thank Drs. W. J. Adelman, Jr., David E. Goldman, and R. A. Sjodin for helpful discussions. Acknowledgment is also made to the authors and editors of the *Journal of Physiology* for permission to reproduce several figures, and to Mrs. Louise Dwyer for carrying out the digital computations. This work was supported in part by U.S. Public Health Service Grant HB07285.

Received for publication 12 May 1967 and in revised form 5 June 1968.

REFERENCES

1. HODGKIN, A. L., and A. F. HUXLEY. 1952. *J. Physiol.* (*London*). **117**:500.
2. MULLINS, L. J. 1960. *J. Gen. Physiol.* **43**(May Suppl.):105.
3. HOYT, R. C. 1963. *Biophys. J.* **3**:399.
4. GOLDMAN, D. E. 1964. *Biophys. J.* **4**:167.
5. CHANDLER, W. K., A. L. HODGKIN, and H. MEVES. 1965. *J. Physiol.* (*London*). **180**:821.
6. CHANDLER, W. K., and H. MEVES. 1966. *J. Physiol.* (*London*). **186**:121P.
7. ADELMAN, W. J., JR., and J. P. SENFT. 1966. *Nature.* **212**:614.
8. ADELMAN, W. J., JR., and Y. B. FOK. 1964. *J. Cellular Physiol.* **64**:429.
9. CHANDLER, W. K., and H. MEVES. 1965. *J. Physiol.* (*London*). **180**:788.
10. FRANKENHAEUSER, B. 1959. *J. Physiol.* (*London*). **148**:671.
11. NOBLE, D. 1962. *J. Physiol.* (*London*). **160**:317.
12. FRANKENHAEUSER, B. 1960. *J. Physiol.* (*London*). **151**:491.